Experimental and Numerical Modelling of Landslide-Generated Tsunamis

C.N. Whittaker [1], R.I. Nokes [1] and M. Davidson [1]

[1]Department of Civil and Natural Resources Engineering
University of Canterbury, Christchurch 8140, New Zealand

Abstract

An experimental and numerical investigation into the generation and propagation of landslide-generated tsunamis is presented. In the physical experiments, the landslide is modelled as a solid block moving along a horizontal boundary in a long flume. A mechanical system is used to control the landslide motion, and an application of the laser-induced fluorescence method is used to measure free surface elevations.

The amplitude of waves generated during experiments are compared to those predicted by a semi-analytical model. This model is based on inviscid-irrotational theory, and is computationally inexpensive.

Results show that the semi-analytical model effectively predicts the phase and speed of the generated waves, but slightly under-predicts their amplitude. An increase in landslide Fr has a greater effect on the wave amplitude and energy than an increase in the initial acceleration of the landslide.

Introduction

Tsunamis pose a significant hazard to communities in coastal zones, especially within countries in seismically active regions of the world. As populations increase, human development in coastal areas is expected to increase, putting more people and infrastructural assets in danger from tsunami events. Anticipated sea level changes due to climate change may further increase the vulnerability of low-lying coastal regions to tsunamis and other large-wave events.

Several different types of tsunami exist; these are classified by their source mechanism. Two common types are those caused by coseismic displacement of the seafloor and those caused by a landslide (either initiated above or below the water surface level). In general, coseismic tsunamis tend to have lower initial amplitudes, but much longer wavelengths, than landslide-generated tsunamis, due to the different horizontal and vertical scales of the forcing mechanisms of the types of waves [3]. Thus landslide-generated tsunamis tend to be more dangerous to communities in the vicinity of the landslide, due to their large wave heights and short warning times, but they do not possess the same potential for transoceanic devastation as coseismic tsunamis. Landslide-generated tsunamis can additionally be triggered in inland water bodies, such as alpine lakes.

Previous efforts in studying landslide-generated tsunamis can be divided into three broad categories; observation, prediction and replication. Observations are taken in field situations after a tsunami event, and can include measurements of run-up levels, interviews with eyewitnesses regarding the timing of the event, and other specific measures of interest, such as levels of damage and bathymetric effects. Predictive models form an important part of tsunami warning systems, as these can give an indication of the expected wave properties based on a particular initial wave forcing. Replication in the laboratory allows calibration of these predictive models, to ensure that they can adequately describe the physics of an idealised problem.

Project objectives

This project focuses on the replication and prediction phases of research into landslide-generated tsunamis. Past experimental studies in this field have typically used a solid block to simulate a submarine landslide, for example Watts [4]. This solid block moved down an inclined plane under the influence of gravity, generating waves which propagated in both the onshore and offshore directions. The main issues with this methodology are that wave properties in the onshore direction could not be measured, and the range of landslide motion was limited.

This project aims to perform a series of experiments in which a submarine landslide is modelled as a solid block moving along a horizontal boundary beneath fluid of a given depth. The use of a horizontal bottom boundary will allow the properties of both onshore- and offshore-propagating waves to be measured. A mechanical system controls the motion of the landslide, allowing a broader range of motion to be investigated than previously possible. This mechanical system also enables greater experimental repeatability. Results will be compared to the predictions of a two-dimensional semi-analytical model [1].

Experimental Methodology

All experiments were carried out in a flume of length 14.66 m, width 0.25 m and working depth 0.505 m. This depth was reduced by 0.08 m due to the installation of a false floor within the flume. This false floor was constructed from aluminium plate, containing a 10 mm slot, to provide a suitable sliding surface for the landslide block in the central 5 metres of the flume. The outer sections were constructed from acrylic of 12 mm thickness. A schematic of the setup used to simulate a tsunami generated by submarine landslide in the laboratory is provided in figure 1.

The landslide was modelled as a solid aluminium block, of dimensions 0.5 m length, 0.25 m width and 0.026 m thickness. It was semi-elliptical in shape. A mechanical system moved the block along the horizontal sliding surface of the false floor. The motion of the landslide block generated free surface disturbances, which were measured using an application of the laser-induced fluorescence method, as used in [1] and [2]. Since the camera's field of view was limited, data for the wave-field contained within the entire flume could only be recorded by repeating each experiment multiple times.
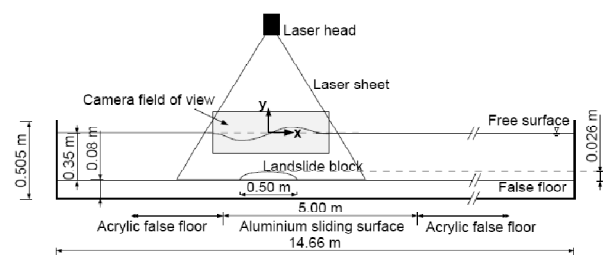

Figure 1. Schematic of experimental setup used in two-dimensional laser-induced fluorescence experiments.

Landslide motion control

Since experiments needed to be repeated multiple times (37 in total) to gain a full LIF dataset, repeatability of landslide motion was a requirement of the system. The mechanical system used to provide this landslide motion was housed beneath the false floor in the base of the flume, as shown in figure 2. This system consisted of a servo motor (located outside of the flume), two toothed timing belts, an aluminium I-section connector, and an acrylic base plate.
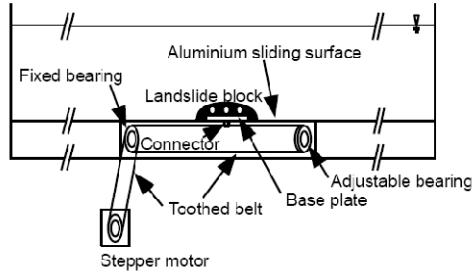
Figure 2. Components of the mechanical system used to provide motion to the landslide block.

A recess was milled into the base of the landslide block so that it could rest on the base plate with approximately 1 mm clearance from the sliding surface. As a safety precaution, a magnet was inserted into the base plate to enable motion shutoff if the block passed over limit switches located at either end of the sliding surface.

The base plate was connected to the toothed timing belt, located beneath the slotted sliding surface, by an aluminium I-section. The belt ran between two stainless steel self-aligning bearings. The adjustable bearing was able to be moved and locked in place to keep the belt at the correct tension and alignment. The fixed bearing penetrated the flume wall and a mechanical lip seal was used to ensure that the flume remained water-tight. A smaller toothed timing belt connected the fixed bearing to the motor.

The motor was a BL86-660 Watt brushless servo motor, of the kind used in CNC machines. This motor was connected to a drive system, and accepted input from a computer terminal. Motion was specified within the control program in the form of a csv file containing a series of displacement-time targets (where displacements were relative to a 'home' position at the left end of the sliding surface). The motor was controlled in steps, at a gearing of 31,250 steps per linear metre of landslide motion.

Particle tracking velocimetry checks on landslide motion

To ensure that the mechanical system achieved its velocity targets with good experimental repeatability, a series of PTV experiments were carried out. Three white dots were painted on the side of the landslide block (which was painted matte black, see figure 2). An experimental run was carried out with the camera focused on the side of the landslide block, and the locations of these dots were recorded during the experiment. The motion of the block consisted of three phases; a period of constant acceleration, a period of constant velocity, and a period of constant deceleration. The acceleration was defined by the nondimensional parameter λ and the constant velocity defined by the landslide Fr, as stated in equation (1). The other governing parameter defined in equation (1) is the nondimensional water depth, τ. A schematic showing the dimensional variables D and L_b is shown in figure 4.

$$\lambda = \frac{a_0}{g} \quad , \quad Fr = \frac{u_{max}}{\sqrt{gD}} \quad , \quad \tau = \frac{D}{L_b} \tag{1}$$

Due to the limited horizontal extent of the camera's field of view (approximately 400 mm), multiple camera locations were used to capture the complete range of motion of the block. To ensure that the start time of motion was able to be recorded, a light-emitting diode (LED) was programmed to flash for approximately 0.1 s upon initiation of landslide motion via the control program. This LED was then placed within the camera field of view, so that images from different camera locations could be synchronised.

The locations of each dot on the landslide block were identified and subsequently tracked between frames using the Streams© software package. This allowed calculation of the Lagrangian velocities of each dot, which are compared to their target values in figure 3. Time scales are nondimensionalised by the gravitational acceleration, g, and the length of the landslide block, L_b. Length scales are nondimensionalised by the length of the landslide block, L_b.
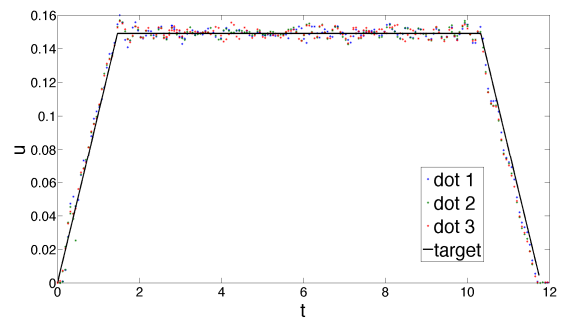
Figure 3. Lagrangian velocity plot of a PTV run with the parameters $\tau = 0.35$, $\lambda = 0.102$, and Fr = 0.25, quantities calculated in equation (1).

Free surface identification using laser-induced fluorescence

In experimental studies of landslide-generated tsunamis, the accurate identification of the spatial and temporal variations in free surface level is very important. These experiments used laser-induced fluorescence (LIF) to achieve this.

The flume was filled with water mixed with a small amount (0.1 mg/L) of Rhodamine B fluorescent dye. A laser sheet illuminated a 2D section of the flume (as shown in figure 1). This meant that the interface between the (bright) water and (dark) air was clearly visible in the plane of the laser sheet. An orange filter was placed in front of the camera to remove the light emitted by the laser, allowing the fluoresced light to pass.

A camera was positioned 2.1 m from the sidewall of the flume, and observed the free surface at a downward angle of approximately 5°. This allowed the interface between the air and water to be recorded in the plane of the laser sheet without interference from the meniscus at the near flume sidewall. A total of 37 locations were recorded, and the camera was mounted on a computer-controlled gantry, which used a similar mechanical system to the landslide block to ensure accurate positioning. Images were synchronised between camera locations using a light-emitting diode (LED) in the same manner as during the PTV tests.

After recording, images were processed to construct the free surface record. Three main steps were used to determine the free surface within the recorded images: Intensity field calculation, interface identification using a threshold intensity value, and combination of the free surface record from different camera locations. The first step was carried out in the Streams© software package, and second and third steps were carried out in the computer program MATLAB. The resulting free surface profile was validated against wave gauge measurements at specific locations within the flume, with excellent agreement.

Semi-analytical model

Results of experiments were used to validate the predictions of a semi-analytical model. This model simulated the waves generated by a solid landslide block moving along a horizontal bottom boundary within a fluid of constant depth. The domain and associated variables used in numerical simulations are shown in figure 4. The landslide block had length L_b and thickness h_b, and moved in the positive x-direction. The fluid had constant depth D when at rest; free surface disturbances due to landslide motion were represented by the variable η.
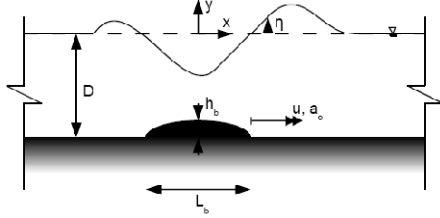

Figure 4. Problem domain used in spectral model formulation. The domain is infinite in horizontal extent, and the landslide moves in the positive x-direction. The origin is located on the undisturbed free surface, directly above the location of the landslide centre of mass.

The fluid is assumed to be inviscid, and all fluid motions are assumed to be irrotational. Due to these assumptions, the governing equation of this problem is Laplace's equation for the velocity potential.

This problem was formulated and solved in nondimensional form. Length scales were nondimensionalised by the length of the landslide block, L_b. Times, were nondimensionalised by the gravitational acceleration, g, and landslide block length, L_b. Perturbations to the system (e.g. η on the free surface) were nondimensionalised by the thickness of the landslide block, h_b. Due to the use of the linear assumption, the boundary conditions were applied on y = -D and y = 0, instead of on the actual boundaries which included the slider shape and perturbed free surface.

The assumed solution form for the free surface displacement, $\eta(x,t)$, based on a spectral decomposition of wave modes, is given in equation (2). In this equation the variable k is the wavenumber, ω is the angular frequency of the waves, and $c(k,t)$ are spectral coefficients.

$$\eta(x,t) = \int_{-\infty}^{\infty} e^{i(kx-\omega t)} c(k,t)dk \qquad (2)$$

The shape of the landslide block is also expressed in terms of a Fourier decomposition with components $p(k)$. This Fourier decomposition is stated in equation (3), where θ is a local coordinate relative to the position of the landslide centre of mass, and $f(\theta)$ is the height of the landslide above the bottom boundary.

$$\frac{\partial f}{\partial \theta} = \int_{-\infty}^{\infty} e^{ik\theta} p(k)dk \qquad (3)$$

The governing equations for the spectral coefficients $c(k,t)$ are given in equations (4) and (5), where $K(k,t)$ is the forcing function associated with the motion of the landslide. In equation (5), τ is the depth parameter, $\tau = D/L_b$, ρ is the landslide thickness parameter, $\rho = h_b/L_b$, and x_0 is the position of the landslide centre of mass. Since solutions are linearly independent in k, equation (4) is expressed as an ODE in t, with k as a parameter, and solved at each k.

$$\frac{d^2c(k,t)}{dt^2} - 2i\omega\frac{dc(k,t)}{dt} + K(k,t) = 0 \qquad (4)$$

$$K(k,t) = \frac{\rho p(k)e^{i(\omega t - kx_0)}}{\cosh(k\tau)}\left(\frac{d^2x_0}{dt^2} - ik\left(\frac{dx_0}{dt}\right)^2\right) \qquad (5)$$

The solution for the wave amplitude $\eta(x,t)$ had two steps; solving the ordinary differential equation (ODE) stated in equation (4) for the spectral coefficients $c(k,t)$ and then numerically integrating these coefficients using equation (2) to solve for $\eta(x,t)$. The first step was achieved by expressing equation (4) as a system of two first-order ODEs and solving the system of equations for $c(k,t)$ over a range of k-values. The numerical solution of the problem was carried out in the computer program MATLAB. The predictions of the wave amplitudes from this model are compared to experimental results in the following section.

Results and discussion

Three different parameters were varied during the experimental and numerical simulations of landslide-generated tsunamis. These parameters were the landslide submergence depth, the initial acceleration of the landslide block and the landslide Froude number, as defined in equation (1). The parameter space investigated during simulations is provided in table 1. In each simulation, the constant velocity regime, defined by the landslide Froude number, lasted for t = 8.86 nondimensional time units. The reason for selecting a fixed time at constant velocity was because there was a limited time before the waves reached the ends of the flume during experiments, and the reflections from these waves effectively ended the experiment.

τ	λ	Fr
0.35	0.051	0.125
0.70	0.102	0.250
	0.153	0.500

Table 1. Parameter space explored during simulations. Fr is given as a nondimensional measure of the maximum landslide velocity.

A contour plot of the waves generated during a typical experiment ($\tau = 0.70$, $\lambda = 0.102$, Fr = 0.25) is shown in figure 5. Initially the landslide motion generated a crest in the offshore direction and a trough in the onshore direction. The amplitude of the initial offshore propagating crest is larger than the amplitude of the initial onshore-propagating trough. The low-pressure region above the landslide block has the effect of adding energy to the wave-field if it is located beneath a trough, and removing energy from the wave-field if it is located beneath a crest. Troughs generated in the offshore direction therefore increased in amplitude while they interacted with the landslide. In this experimental run the landslide Froude number was 0.25, so the velocity of a free wave in the channel was approximately four times faster than the maximum velocity of the landslide block. This limited the duration of the interaction between each offshore-propagating trough and the landslide block, and after this short period of interaction these waves would propagate at the free wave speed. Because the phase velocity of these waves was greater than the group velocity, waves were created at the back of each wave packet.

The large offshore-propagating trough and onshore-propagating crest at approximately t = 12 are the result of the deceleration period in the landslide motion. These waves are of interest because the large onshore-propagating crest is most likely to cause inundation of coastal communities. Figures 6–9 show comparisons between the numerical predictions and experimental measurements of wave amplitudes during the experiments.
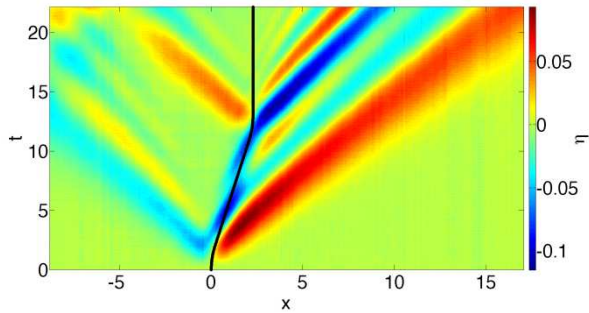
Figure 5. Contour plot of the wave-field generated during an experimental run, with τ = 0.70, λ = 0.102, Fr = 0.25. The reflection of the initial onshore-propagating trough from the end of the flume is visible after t = 15. The landslide centre-of-mass position is shown as a black line.
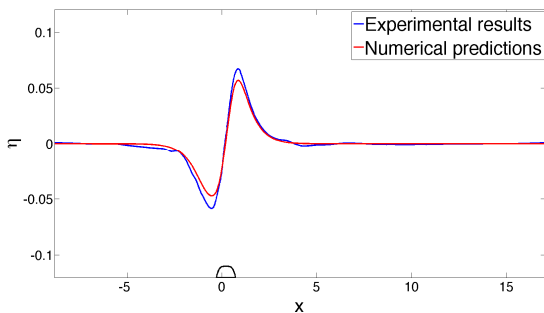

Figure 6. Wave-field plot at nondimensional time t = 2, at the end of the acceleration phase of motion. The landslide motion has generated a crest in the offshore direction and a trough in the onshore direction.
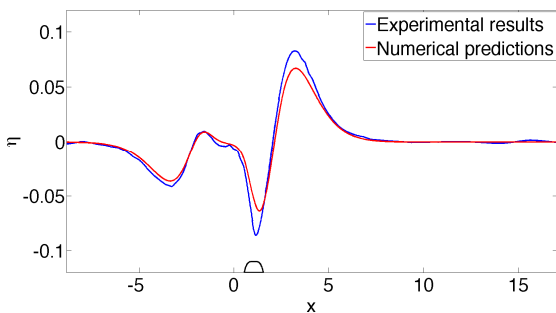

Figure 7. Wave-field plot at nondimensional time t = 6, during the constant velocity phase of motion. The second crest in the onshore direction is now visible. The offshore trough has increased in amplitude, while the offshore crest has decreased slightly in amplitude.
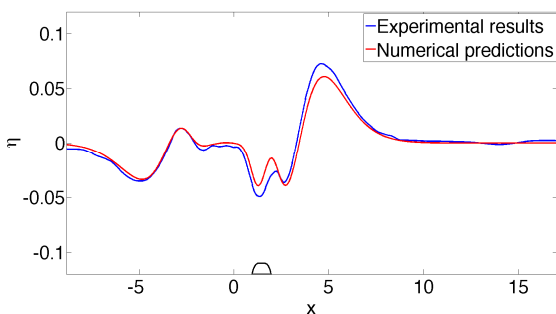

Figure 8. Wave-field plot at nondimensional time t = 8, also during the constant velocity phase of motion. The first offshore trough has begun to move away from the landslide block, and the next trough starts to interact with the landslide block.
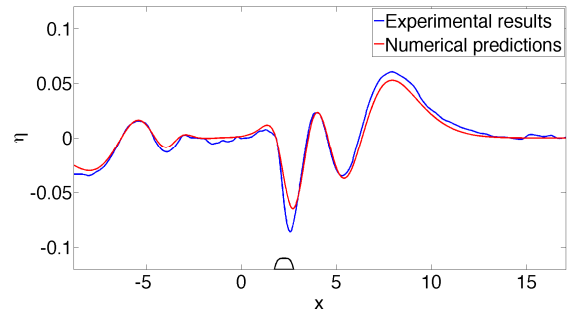

Figure 9. Wavefield plot at time t = 12, during the deceleration phase of motion. A large trough has formed above the landslide block, and the onshore-propagating crest is beginning to be formed beside it.

Figures 6–9 show that the semi-analytical model is effective at predicting the phase and speed of the generated waves, although it under-predicts the amplitudes of the waves by approximately 10%. This result is somewhat counter-intuitive, as the inviscid-irrotational model does not account for fluid viscosity or the turbulent wake behind the landslide block, and these were expected to remove energy from the wave-field. Ongoing work is being carried out to verify this discrepancy using an independent numerical model.

The results and comparisons shown in figures 6–9 are based on only one combination of λ, Fr, and τ. In total 18 runs were carried out, with a range of these parameters. In qualitative terms, the effect of increasing the depth was to decrease the amplitude of generated waves. The decrease in amplitude was proportional to the increase in depth. An increase in initial landslide acceleration led to a proportional increase in wave amplitude. An increase in landslide Froude number led to an increase in wave amplitude proportional to the square of the Froude number.

Conclusions

The generation and propagation of landslide-generated tsunamis have been investigated using experimental and numerical simulations. The experiments used a mechanical system to model the landslide motion, improving the range and repeatability of the motion able to be modelled, and enabling, for the first time, quantitative measurements of the onshore-propagating wave packet to be made.

The semi-analytical model, based on inviscid flow theory, successfully predicted the phase and speed of the waves generated and measured during the LIF experiments. However, the amplitudes of the experimentally-measured waves were under-predicted by the model.

References

[1] Sue, L.P. (2007), Modelling of tsunami generated by submarine landslides, *PhD Thesis, University of Canterbury, New Zealand*.

[2] Sue, L.P., Nokes, R.I., Davidson, M.J. (2011) Tsunami generation by submarine landslide: Comparison of physical and numerical models, *Environmental Fluid Mechanics*, **11** (2), 133-165.

[3] Synolakis, C.E., Bardet, J.-P., Borrero, J.C., Davies, H.L., Okal, E.A., Silver, E.A., Sweet, S., Tappin, D.R. (2002), The Slump Origin of the 1998 Papua New Guinea Tsunami, *Proceedings: Mathematical, Physical and Engineering Sciences.*, **458** (2020), 763-789.

[4] Watts, P. (2000), Tsunami Features of Solid Block Underwater Landslides, *Journal of Waterway, Port, Coastal, and Ocean Engineering*, **126** (3), 144-152.